

## Article

# Investigation into Occurrence Mechanism of Rock Burst Induced by Water Drainage in Deep Mines

Bo Wang<sup>1,2,3,4</sup> , Guorui Feng<sup>1,3,\*</sup>, Fuxing Jiang<sup>4</sup>, Junpeng Ma<sup>2</sup>, Chao Wang<sup>2</sup>, Zhu Li<sup>1,3</sup> and Wenda Wu<sup>1,3</sup>

<sup>1</sup> College of Mining Technology, Taiyuan University of Technology, Taiyuan 030024, China; wangbo01@tyut.edu.cn (B.W.); lizhu01@tyut.edu.cn (Z.L.); wuwenda@tyut.edu.cn (W.W.)

<sup>2</sup> Yankuang Energy Group Co., Ltd., Jining 273500, China; ykmajunpeng@163.com (J.M.); ykwc123@163.com (C.W.)

<sup>3</sup> Key Laboratory of Shanxi Province for Mine Rock Strata Control and Disaster Prevention, Taiyuan 030024, China

<sup>4</sup> School of Civil and Resource Engineering, University of Science and Technology Beijing, Beijing 100083, China; jiangfuxing@163.com

\* Correspondence: fgrpaper\_tyut@126.com

**Abstract:** Confined aquifers widely exist in the strata of the Ordos mining area. Water drainage before mining is an effective measure to avoid water inrush disasters caused by the connectivity between mining-induced roof fractures and aquifers. However, rock burst disasters occur frequently in the mining process of many water drainage working faces. The statistics show that the surrounding rock of nine water drainage working faces in five mines has suffered different degrees of rock burst, which seriously restricts the safe, efficient production and sustainable development of ten-million-ton modern mines in China. Based on this, taking the 22,106 longwall working face (LW22106) of the Shilawusu Mine, Ordos, as the engineering background, this paper investigates the occurrence mechanism of water drainage on rock burst in the roof water-rich area by using theoretical analysis, similar material simulation, microseismic measurement and other methods. The main conclusions are as follows: (1) After the drainage of the water-rich area, the pressure relief zone, pressurized zone and pressure stabilization zone are formed in sequence from the center to both sides. The width of the pressure relief zone is consistent with that of the water-rich area, and the width of the pressurized zone is about 35 m on one side. (2) When the mining is passing the pressurized zone, the coal rock mass is under the joint influence of gravity stress, mining disturbance stress and drainage transfer stress. The superimposed stress generally exceeds 2.5 times the uniaxial compressive strength (UCS) of the coal rock mass, and the maximum reaches 3.24 times, far exceeding the critical value of rock burst (1.5 times UCS), which is the main reason to induce rock burst. (3) The dynamic change in the rock burst risk areas before and after drainage in water-rich area no. 4 has been predicted, and the number of risk areas increases from 4 before drainage to 13 after drainage. Since the stress superposition effect differs due to different mining speeds, it is proposed that the dynamic regulation of mining speed in the front and at the back of the drainage area is an effective and efficient method for rock burst prevention and control. The research results will provide a theoretical basis and technical support for the prevention and control in the roof water-rich area of deep mines.

**Keywords:** deep mining; water drainage; rock burst; stress distribution; classification of risk areas



**Citation:** Wang, B.; Feng, G.; Jiang, F.; Ma, J.; Wang, C.; Li, Z.; Wu, W. Investigation into Occurrence Mechanism of Rock Burst Induced by Water Drainage in Deep Mines. *Sustainability* **2023**, *15*, 8891. <https://doi.org/10.3390/su15118891>

Academic Editor: Cun Zhang

Received: 7 May 2023

Revised: 27 May 2023

Accepted: 29 May 2023

Published: 31 May 2023



**Copyright:** © 2023 by the authors. Licensee MDPI, Basel, Switzerland. This article is an open access article distributed under the terms and conditions of the Creative Commons Attribution (CC BY) license (<https://creativecommons.org/licenses/by/4.0/>).

## 1. Introduction

With the gradual depletion of shallow coal resources in China, coal resource exploitation presents a deep mining tendency, and deep mining is increasingly becoming normal [1,2]. After coal mines step into the deep mining stage, geological conditions and stope structures become much more complex, the occurrence frequency and damage degree of dynamic disasters remarkably increase, and more and more mines will be faced with the threat of dynamic disasters such as rock burst [3–6]. Since 2010, 25 rock burst accidents

have occurred in China, resulting in 119 deaths and 108 injuries. Rock burst has become a key scientific problem and a worldwide problem that needs to be solved urgently [7–11].

Ordos coalfield, as an important coal base in China, stretches across Shaanxi, Gansu, Ningxia, Inner Mongolia and Shanxi provinces, as shown in Figure 1. Group Yan'an and Group Zhiluo artesian aquifers widely exist in the coal seam roof, and the large water-rich areas serve as the direct water source for coal seam mining [12]. In the mining process on the working face below the roof water-rich areas, roof disasters such as water inrush and sand bursting may be faced [13]. In order to avoid the roof water inrush and reduce the preparation time on the working face, the roof water drainage should be carried out during excavation on the working face. However, the drainage in the water-rich area causes the stress redistribution of the coal seam and roof [14], forming a stress concentration area and increasing the possibility of rock burst. In recent years, rock burst has appeared several times in the mining process of some roof water drainage working faces, which seriously restricts the safe and efficient production and coal supply. Therefore, the investigation into the influence mechanism of roof water drainage on the stress distribution of overlying rock is of great significance to reveal the occurrence mechanism of rock burst on the water drainage working face in the Ordos mining area, take measures for rock burst prevention and control and ensure the safety of the working face.

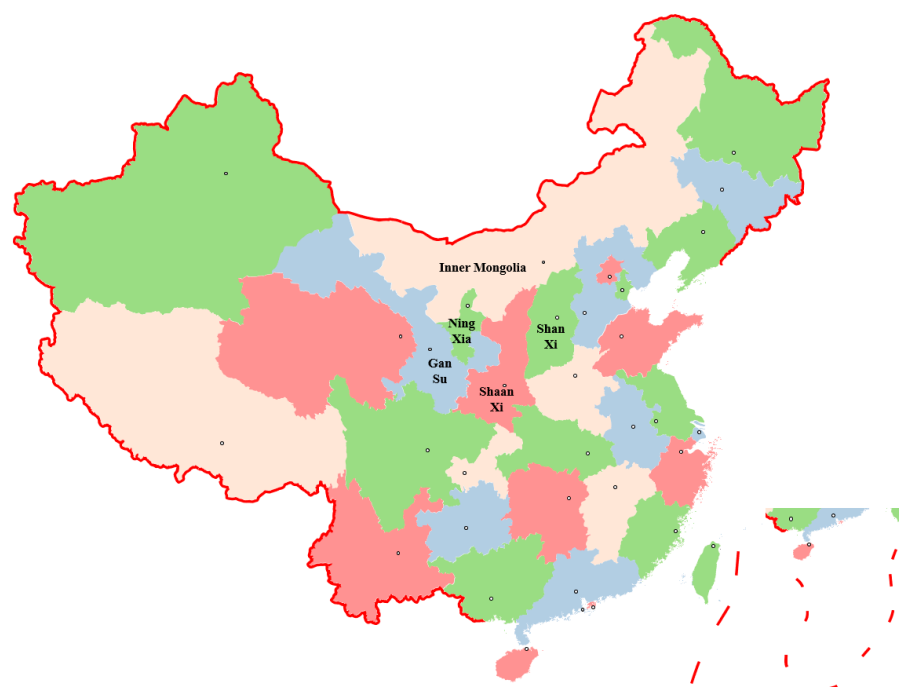


**Figure 1.** Location map of Ordos coal base in China.

Field practice shows that rock burst is affected by many factors, including geological and mining factors. Researchers have conducted extensive studies on the influencing factors of rock burst and made rich scientific research achievements. Jiang et al. [2,15] believed that rock burst, affected by various inducing factors, was a nonlinear dynamic process in the deformation of the coal rock mass system under different geological conditions and mining environments. During the process, energy stored in a stable state was transformed into energy released in an unstable state. They also pointed out that the essence of rock burst was the stress-induced sudden instability and failure of the coal rock mass. Dou et al. [16,17] and Cai et al. [18] held that rock burst was closely related to the physical and mechanical properties of coal rock, as well as the static and dynamic loads on coal rock. Based on this, they further investigated the energy and stress conditions of rock burst induced by dynamic and static loads and clarified the mechanism and two types of rock burst induced by static and dynamic loads: high static load type and strong dynamic load type. Qi et al. [19]

explained many determining factors for the occurrence of rock burst and put forward the idea of multi-scale and multi-source prevention and control of dynamic disasters in deep coals. Jiang et al. [20] and Zhu et al. [21,22] found that gravity and tectonic stress were the foundation stress of determining the rock burst in the stope, and the stress generated by the movement of overlying strata was the force source that induces the rock burst. They believed that the variable structure forms and movement laws of overlying strata were the main reasons for the complex mechanism and various forms of rock burst and finally raised the technical idea of classification evaluation on rock burst. Zhao et al. [23] studied the loading characteristics and instability mechanism of gob-side roadway in deep mining and revealed the “three-load” superimposition rock-burst-inducing mechanism of gob-side roadway under the influence of lateral static load, advanced static load and disturbance dynamic load in goaf. Cao et al. [24–26] conducted an investigation into the stress distribution law and multi-dimensional information of microseismic events near the residual coal pillar, holding that the residual coal pillar was the main influencing factor of rock burst.

In terms of the studies on the relationship between mining disturbance and rock burst, Gong et al. [27,28] found that the critical loading rate obviously existed in the coal–rock combined body, and the mutation rate of rock burst tendency was relatively obvious near the critical loading rate. Zhao et al. [29] illustrated the mechanism of roof energy accumulation and release under the influence of mining speed, believing that the increase in roof energy accumulation was essentially the increase in loading rate when the mining speed changed from slow to fast. Huang et al. [30] conducted uniaxial compression tests on the coal–rock combined body under different loading rates, explaining that the loading rate had a huge effect on failure forms and the rock burst tendency of coal rocks. Cui et al. [31] evaluated the rock burst risk of a coal body under different mining strengths and revealed the mining disturbance characteristics on the working face of deep coal seams under different mining strengths. Feng et al. [32] adopted theoretical analysis and microseismic monitoring to reveal how mining speed influenced the energy released by the movement of the hard roof, indicating that the energy from the hard roof breaking presented an obvious positive correlation with the mining speed. In the aspect of drainage-induced rock burst, scholars have conducted some research studies on the effect of water on the physical and mechanical properties of coal rock, but few studies focus on how drainage affects the stress field of coal and rock. Zhou et al. [33] explored the mechanical behavior of coal samples during water saturation, finding that when the coal around the mining space was subjected to water, the high degree of water saturation in the coal decreased the risks of coal bursts significantly. Zheng et al. [34] pointed out that there was a negative correlation between the compressive strength of coal and soaking time by studying the influence of soaking time on the macro and micro mechanical properties of coal samples. Zhang et al. [35–37] focused on the water weakening of rock strength and its influencing factors (water content, immersion time and wetting–drying cycles), and they found that the strength of the rock mass decreases to varying degrees with water content, immersion time and wetting–drying cycles depending on the rock mass type and mineral composition.

It can be found that the existing rock burst theories usually ignore water drainage as an inducing factor of rock burst, which leads to the lack of reliability and accuracy in the classification of rock burst risk areas on the working face with the roof water-rich areas and the absence of targeted prevention measures. For example, the serious rock burst accident in the drainage lane and no. 3 contact lane of LW1303 in Shandong Longyun Mining Company on 20 October 2018 caused 21 deaths [5] and damaged a 348 m roadway, including a 198 m severely damaged section, as shown in Figure 2. According to the accident investigation report, the influence of roof water drainage on the regional stress distribution was one of the indirect causes. The result showed that roof water drainage was one of the induced factors of rock burst in Ordos deep mining area.

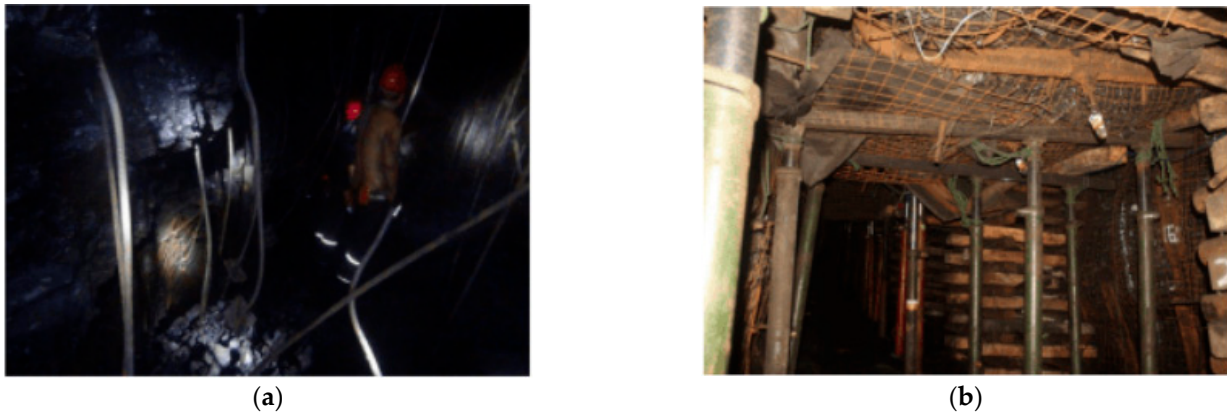


**Figure 2.** Scene damage of 20 October rock burst accident in Longyun Mine: (a) Anchor bolt bent and suspended; (b) Two sides convergence, roof subsidence.

In view of this, taking LW22106 of the Shilawusu Mine in Ordos as the engineering background, this paper adopts theoretical analysis, similar material simulation and micro-seismic monitoring to investigate the occurrence mechanism of water drainage on rock burst in the roof water-rich area of deep mines and reclassified the risk areas on the working face, attempting to predict the rock burst risk more accurately. The research results can provide a theoretical basis and technical support for safe and efficient mining on the roof water-rich working face in the Ordos mining area.

## 2. Engineering Background

### 2.1. Field Conditions of LW22106

The Shilawusu Mine, located in the Ordos mining area, is mainly mining the 2-2 coal seam, whose coal seam, roof and floor have a weak rock burst tendency. LW22106, with a width of 300 m and a length of 1120 m, is the first mining face of the south wing in the 221 mining area, and a strike longwall full-mechanized coal caving method is adopted for mining on this working face. The average surface elevation is 1340 m, the average mining depth is 660 m, and the average coal thickness is 9.02 m. Like a flat seam, the 2-2 coal seam has a simple geological structure. The immediate roof of the 2-2 coal seam is 0.77 m thick mudstone, the basic roof is 31.26 m thick fine sandstone, the direct bottom is 6.10 m thick sandy mudstone, and the basic bottom is 9.25 m thick siltstone. According to the hydrogeological exploration results, there is a Group Zhiluo artesian aquifer with an average thickness of 110 m at 39.65~62.65 m and an average of 50.52 m above LW22106 of the 2-2 coal seam. The water-rich areas are unevenly distributed above the working face. The specific numbers and spatial distribution locations of the four water-rich areas are shown in Figure 3.

During the mining process on the working face, the water drainage has been carried out through drainage holes. Specifically speaking, the drilling fields and the drainage holes are intensively arranged in the vicinity of the water-rich area, with one drilling field for every 200 m. The diameter of drilling holes for roof water drainage is 91 mm, and the final pitch of the holes is less than 80 m. After the drilling is completed, the gate valve and pressure gauge are installed at the orifice. The gate valve is connected with the drainage pipe and flowmeter for drainage water until the water pressure in the water-rich area is reduced up to the safety mining standard, which is that roof water disasters such as water inrush and sand bursting will not occur in the mining process. The microseismic monitoring system is SOS, developed in Poland [38]. Eight microseismic sensors are arranged around LW22106, among which no. 5 and no. 6 sensors are constantly moved and optimized along with the mining on the working face. These sensors are used to monitor microseismic events in the mining process and capture the precursor information of rock burst.

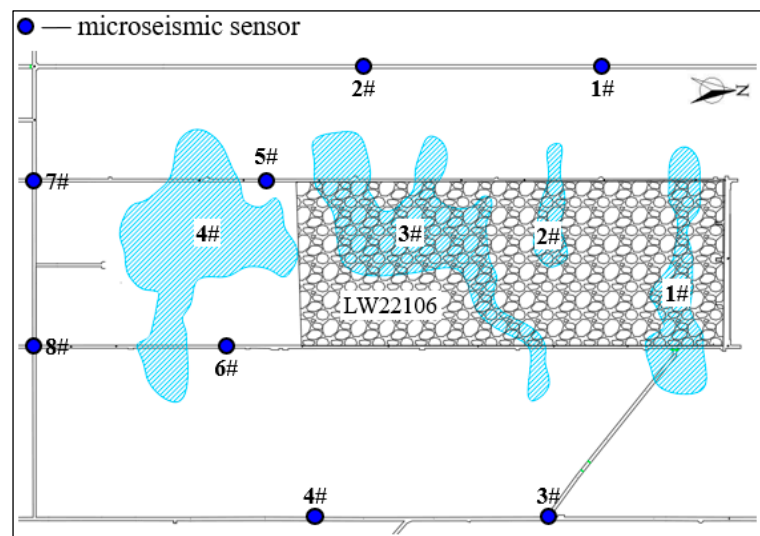


Figure 3. Distribution plan of sandstone water-rich area on roof of LW22106.

### 2.2. Description of Mine Seismicity on the Working Face

At 19:00 on 10 October 2019, the rock burst appeared in the normal mining process of LW21106, and the staff reported the big sound of coal blasting on the site. After further on-site investigation, obvious large rib splitting occurred on the coal wall of the working face, a large amount of slag fell off the roof in front of the working face, and part of the coal body in the roadway wall leaked out from the anchor net. Meanwhile, the SOS microseismic monitoring system monitored a large energy event of  $4.0 \times 10^5$  J (source 1) and another large energy event of  $1.13 \times 10^5$  J (source 2) at 20:06, with a time interval of 66 min. In addition to the sound of coal blasting, there was also a small amount of slag falling off the roof. By comparing the real-time online monitoring results of stress on the working face, it was found that the stress of the two gate roads before and after the incident did not change greatly, and the detection hole of pulverized coal presented a normal amount of drilling cuttings in the field construction. The plane projection and profile projection of the events were shown in Figure 4.

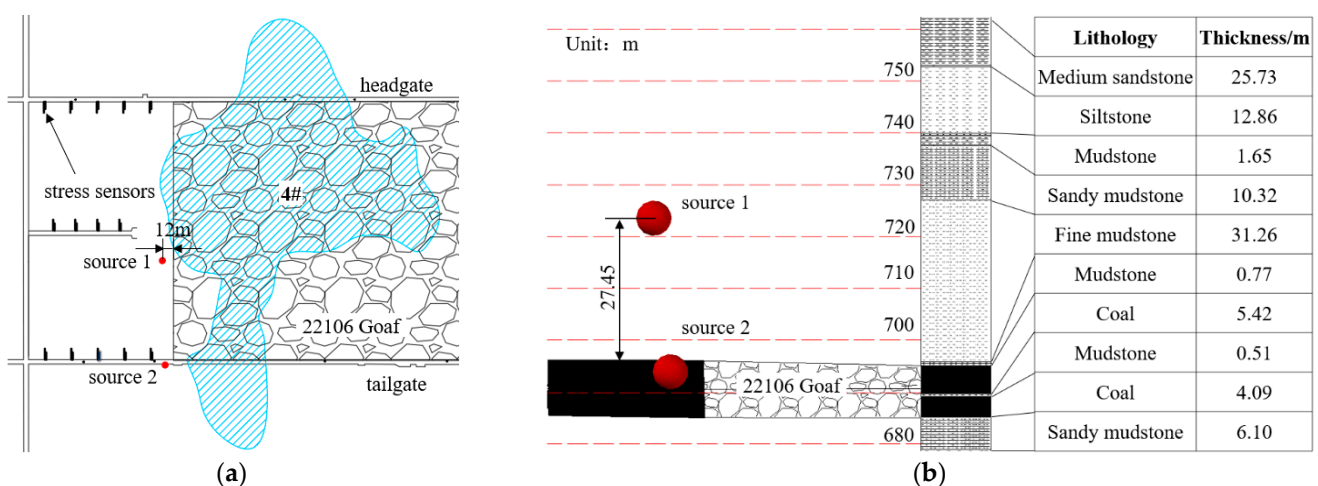


Figure 4. Projection of two microseismic events on 10 October: (a) planar projection; (b) section projection.

As can be seen from Figure 4, Source 1 was horizontally located 12 m in front of the working face and at the edge of the no. 4 water-rich area and vertically located in the basic roof (fine sandstone) above the coal seam with 27.45 m away from the 2-2 coal roof. Source 2 was located in the coal seam. According to preliminary analysis, the water pressure in the no. 4 rich water area declined from the initial 3 MPa to 0.5 MPa after drainage. The

pressure step interval of LW22106 was 20 m, and the mining speed reached 7.2 m/d on that day. Therefore, it was believed that the main reasons for this rock burst were as follows: the overlying basic roof failed to collapse in time due to the excessively fast mining speed on the working face, thus forming a suspended roof and causing energy accumulation; meanwhile, because of the no. 4 water-rich area on the overlying, a stress concentration appeared near the water-rich area after drainage, which increased the stress above the basic roof, accelerated the fracture of the basic roof and produced a large energy event. Moreover, the energy accumulated in the suspended roof could not be quickly released and stored in the coal body in front of the working face. The coal body above the working face was affected by the superposition of the advanced abatement pressure and the drainage transfer stress. The superimposed stress exceeded the own strength of the coal body, thus resulting in its destruction, cracks and energy release and inducing the rock burst on the working face, such as large rib splitting.

### 3. Mechanism of Rock Burst Induced by Roof Water Drainage

#### 3.1. Principle of Effective Stress

There are irregular water-rich areas in the roof of the upper coal seam in dozens of newly built mines with a mining depth of more than 550 m in Ordos. In order to avoid water inrush and reduce preparation time on the working face during the mining process, the water drainage during mining is equal to a mine for a “quasi-liberating seam” in the water-rich area [39]. The stress decreases in the drainage area and increases at the edge. Therefore, when the working face is advancing to the area affected by drainage, rock burst is more easily induced. It is of great necessity to explore how drainage affects the abutment pressure of the working face.

According to the column chart of the roof strata and the on-site pumping operation, the confined artesian aquifer of Group Zhiluo above the LW22106 coal seam mostly includes medium sandstones and fine sandstones, with the maximum value of confined water pressure up to 3 MPa. The artesian aquifer is saturated with high porosity and permeability, and the confined artesian aquifer of Group Zhiluo meets the principle of effective stress. The principle of effective stress means that the total stress carried by the saturated rock–soil mass is mainly borne by two parts [40]. One is the effective stress, namely the skeleton formed by solid particles, which is transmitted through the contact surface between particles; the other is the pore water pressure, namely the water in the pores. The principle of effective stress can be expressed by Formula (1):

$$\sigma = \sigma' + \mu \quad (1)$$

where  $\sigma$  is the total stress of the saturated rock–soil mass (MPa);  $\sigma'$  is the effective stress (MPa); and  $\mu$  is the pore water pressure (MPa).

The bearing force of the artesian aquifer is borne by rock skeleton and pore water. After the drainage in the water-rich area, the pore water pressure and effective stress of the coal rock strata and the physical and mechanical properties of the coal rock mass will make changes within a certain range, resulting in the regional stress adjustment and redistribution of the coal seam and roof.

#### 3.2. Stress Migration Law in the Process of Drainage

The above analysis demonstrates that the pore water pressure will gradually decrease and the effective stress of the artesian aquifer will change after the drainage in the water-rich area of the roof. The support of the artesian aquifer to the overlying strata will decrease within the drainage range, and the overlying strata will suffer from deformation and subsidence under the influence of its gravity. The rock mass on both sides of the water-rich area will provide the supporting reaction force. That is to say, the overlying strata load originally borne by the pore water pressure in the water-rich area is transferred to both sides of the water-rich area, which causes the stress redistribution of the coal seam and roof strata, further forming the pressure relief zone, pressurized zone and pressure stabilization

zone. To further explain, the stress of the coal seam and roof reduces within the drainage area, the stress concentrates at the edge of the area, and the range not affected by drainage is the initial stress zone.

In order to investigate the influence of drainage on the stress distribution of the coal seam and roof before and after drainage in the water-rich area, taking LW22106 of the Shilawusu Mine in Ordos as an example, a section is made along the strike of the working face, and the corresponding estimation mechanical model of abutment pressure after drainage is established to analyze the stress state above the working face before and after drainage, as shown in Figure 5.

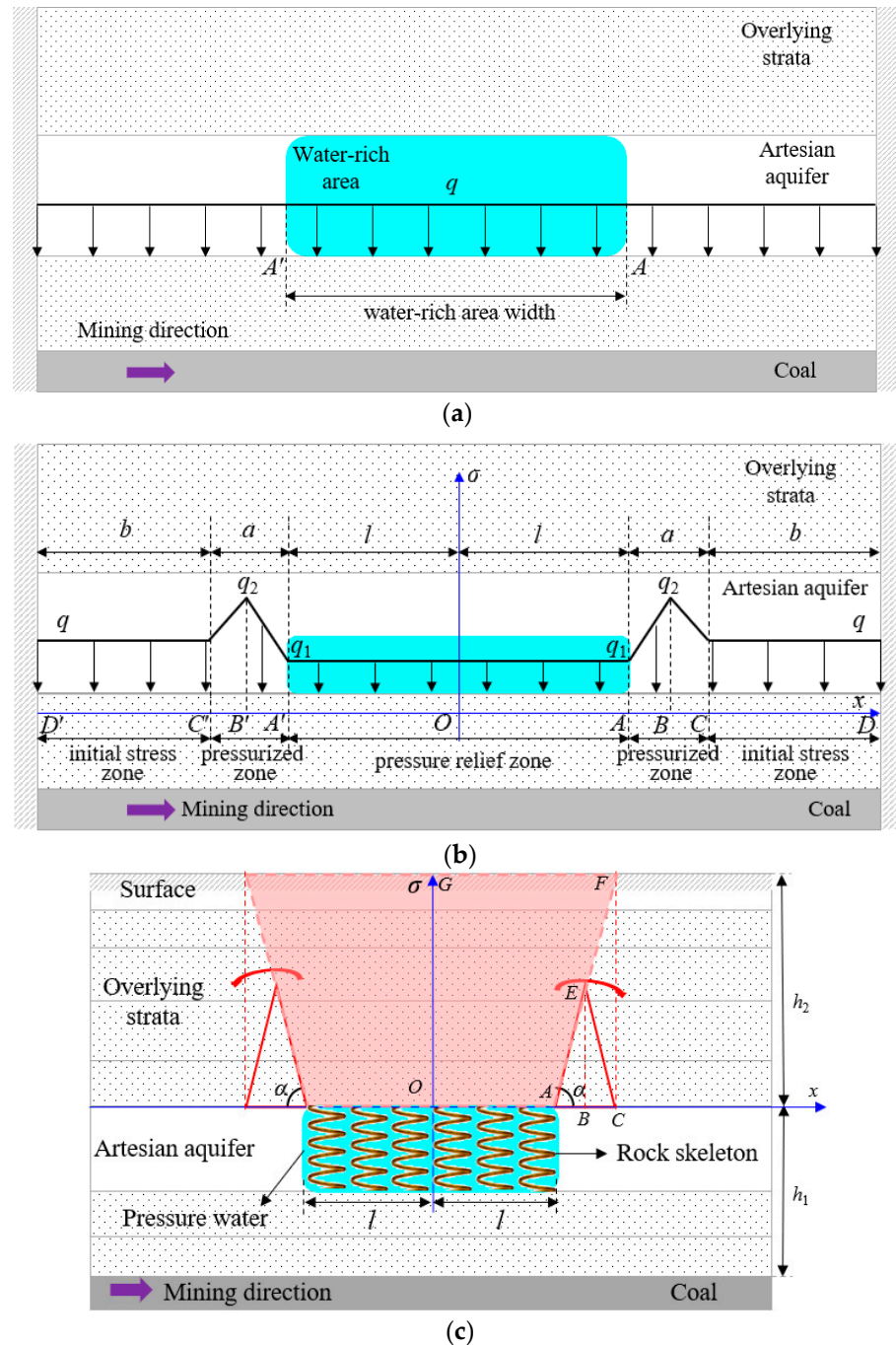


**Figure 5.** Stress distribution state before and after drainage: (a) before drainage; (b) after drainage; and (c) mechanical model for abutment pressure after drainage.

The following assumptions are made for drawing the general law: (1) for the model, the deformation of coal seam and roof strata meets three basic assumptions of material mechanics; (2) for the stress, the water level and water pressure in the area before and after drainage are uniform, all strata are uniformly stressed, and the differences in stress transfer caused by different rock joints are ignored; (3) for the boundary, only an ideal section of the working face is selected for the theoretical analysis because of the irregular shape in the actual water-rich area. In Figure 5a, before the implementation of drainage in the water-rich area, the strata of the artesian aquifer are intact, the overlying strata load  $q$  is uniformly transferred, and the load on the artesian aquifer is the original rock stress. In Figure 5b, the origin  $O$  is the center of the water-rich area. After drainage in the water-rich area, the pore water pressure decreases, forming a pressure relief zone. The support capacity of the upper roof in the drainage range of the water-rich area decreases to  $q_1$  ( $A'A$  section), and the rock mass stress in  $A'C'$  and  $AC$  sections increases, forming a pressurized zone. The stress distribution in the pressurized zone can be simplified into a triangular linear distribution (the maximum stress is  $q_2$ ). The original rock stress in the  $C'D'$  and  $CD$  sections remains unchanged, forming a pressure stabilization zone. Let the length of the  $OA$  ( $OA'$ ) section be  $l$ ,  $AC$  ( $A'C'$ ) section be  $a$  and the  $CD$  ( $C'D'$ ) section be  $b$ , and then the stress distribution in  $D'D$  section is as follows:

$$\sigma(x) = \begin{cases} q & (x \in D'C') \\ \frac{2(q_2-q)}{a}(x+l+\frac{a}{2})+q_2 & (x \in C'B') \\ \frac{2(q_1-q_2)}{a}(x+l)+q_1 & (x \in B'A') \\ q_1 & (x \in A'A) \\ \frac{2(q_2-q_1)}{a}(x-l)+q_1 & (x \in AB) \\ \frac{2(q-q_2)}{a}(x-l-\frac{a}{2})+q_2 & (x \in BC) \\ q & (x \in CD) \end{cases} \quad (2)$$

where  $q$  is the original rock stress (MPa);  $q_1$  is the load in the pressure relief zone after drainage (MPa);  $q_2$  is the maximum load in the pressurized zone (MPa);  $l$  is the half-width of the water-rich area (m);  $a$  is the range of the pressurized zone, expressed as  $a = h_2 / \tan \alpha$  (m); and  $b$  is the range of the pressure stabilization zone (m).

As can be seen from Figure 5 and Formula (2), the stress distribution after drainage is ideally symmetric with respect to the origin  $O$ , which means equal stress is transferred to both sides after drainage. Therefore, it just needs to make a detailed analysis of the stress distribution in the  $OD$  section on the right side of the origin  $O$ , as shown in Figure 5c. In Figure 5c,  $h_1$  is the distance from the top of the artesian aquifer to the coal seam (m);  $h_2$  is the distance from the top of the artesian aquifer to the surface (m); and  $\alpha$  is the displacement angle of overlying strata in the water-rich area caused by drainage. (Compared with mining, the support of the artesian aquifer on its upper strata still exists in spite of a decline in support effect. Moreover, the overlying strata over the aquifer will suffer from fracture bands, but caving bands will not occur or the overlying strata will not stay in a completely overhanging state).

In this model, the water-rich area is simplified to be composed of confined water and a rock skeleton. The rock skeleton can be regarded as an equivalent spring, exerting a supporting reaction force on the overlying strata. The supporting reaction force of the water-rich area on the overlying strata before and after drainage is expressed as:

$$q = \gamma h_2 \quad q_1 = k \gamma h_2 \quad (3)$$

where  $\gamma$  is the rock bulk density ( $\text{kN}/\text{m}^3$ ) and  $k$  is the drainage pressure relief coefficient ( $0 < k < 1$ ), negatively correlated with the drainage degree; that is, the higher degree of the drainage, the smaller the  $k$ .

After drainage, the gravity stress in the overlying OAFG region is transferred to the right of  $\Delta_{ACE}$ , and the transferred weight  $Q_{OAFG}$  can be expressed as:

$$Q_{OAFG} = (2l + \frac{h_2}{\tan \alpha}) \frac{\gamma h_2}{2} - q_1 l \quad (4)$$

Assuming that stress transferred to the lower coal rock mass is approximately an isosceles triangular distribution [20], the load transferred to the right of the OAFG region  $\sigma_{OAFG}$  is as follows:

$$\sigma_{OAFG}(x) = \begin{cases} \frac{2q_2 \tan \alpha}{h_2} (x - l) & (l, l + \frac{h_2}{2 \tan \alpha}] \\ 2q_2 [1 - \frac{\tan \alpha}{h_2} (x - l)] & [l + \frac{h_2}{2 \tan \alpha}, l + \frac{h_2}{\tan \alpha}) \\ 0 & [l + \frac{h_2}{\tan \alpha}, +\infty) \end{cases} \quad (5)$$

where  $x$  is the distance between the transfer stress and the center of the water-rich area. The peak stress transferred from the OAFG region to the pressurized zone  $q_2$  can be expressed as:

$$q_2 = \frac{Q_{OAFG} 2 \tan \alpha}{h_2} = (2l \tan \alpha + h_2) \gamma - \frac{2q_1 l \tan \alpha}{h_2} \quad (6)$$

When the working face is under the water-rich area (pressure relief zone), at the edge of the water-rich area (pressurized zone) and in a more distant area (pressure stabilization zone), the gravity stress of the working face from the overlying strata after drainage differs greatly, which can be expressed as:

$$\sigma_Z(x) = \begin{cases} q_1 + \gamma h_1 & (0, l] \\ (1 - k) \gamma (x - l) \tan \alpha + q_1 + \gamma h_1 & [l, l + \frac{h_2}{\tan \alpha}) \\ \gamma h_1 + \gamma h_2 & [l + \frac{h_2}{\tan \alpha}, +\infty) \end{cases} \quad (7)$$

Based on Formulas (2)–(7), the distribution function of coal seam abutment pressure caused by drainage can be written:

$$\sigma_S(x) = \begin{cases} \gamma h_1 + k \gamma h_2 & (0, l] \\ \frac{2(2l \tan \alpha + h_2 - kl \tan \alpha) \gamma \tan \alpha}{h_2} (x - l) + (1 - k) \gamma (x - l) \tan \alpha + \gamma h_1 + k \gamma h_2 & [l, l + \frac{h_2}{2 \tan \alpha}) \\ 2(2l \tan \alpha + h_2 - kl \tan \alpha) \gamma [1 - \frac{\tan \alpha}{h_2} (x - l)] + (1 - k) \gamma (x - l) \tan \alpha + \gamma h_1 + k \gamma h_2 & [l + \frac{h_2}{2 \tan \alpha}, l + \frac{h_2}{\tan \alpha}) \\ \gamma h_1 + \gamma h_2 & [l + \frac{h_2}{\tan \alpha}, +\infty) \end{cases} \quad (8)$$

As can be seen from Formula (8), the stress concentration caused by drainage shows a negative correlation with the pressure relief coefficient in the water-rich area and is positively correlated with the drainage degree. That is to say, the better the drainage effect, the greater the stress peak in the pressurized zone. According to the research [12,14] and the field observation of water pressure, the water pressure in the rich-water area gradually decreases to the safe mining standard (that is, no water disasters occur, such as water inrush) and eventually tends to be stable with the progress of drainage work. The results show that the stress concentration degree caused by drainage tends to be stable during mining on the working face; the pressure relief zone, pressurized zone and pressure stabilization zone are formed in sequence from the center to both sides; and the pressurized zone applies additional stress to the coal seam and its roof, adding a static stress source for the occurrence of rock burst.

### 3.3. Physical Simulation Verification

Starting from the typical geological conditions of the Ordos mining area, the similarity ratios are determined based on the rock strata condition, physical and mechanical properties of rock [41], geometric size of the test bed and three basic similarity laws. Among them,

the geometric ratio is 1/200, the bulk density ratio is 0.6, the strength ratio is 0.6/200, and the time ratio is 1/14. For the convenience of time simulation, the time ratio is set as 1/12; that is, 2 hours in the experiment equals the on-site 24 h. The model size is 5000 mm (length) × 250 mm (width) × 1680 mm (height). Sand is used as the skeleton material, and calcium carbonate and gypsum are used as cementing materials. Table 1 displays the proportions of similar simulation materials. A pressurized steel plate is arranged at the top of the model, and eight hydraulic jack devices are uniformly arranged above the steel plate to exert vertical forces on the model, which replaces the rock layer above that needs to be simulated.

**Table 1.** Proportion of similar simulation materials.

Serial Number	Lithology	Thickness/cm	Total Thickness/cm	Similar Materials/kg			
				Sand	CaCO <sub>3</sub>	Gypsum	Water
26	Sandy mudstone	5	158	85.23	2.56	5.97	9.38
25	Fine sandstone	4	153	66.67	5.00	3.33	7.50
24	Sandy mudstone	5	149	85.23	2.56	5.97	9.38
23	Fine sandstone	4	144	66.67	5.00	3.33	7.50
22	Siltstone	19	140	316.67	27.71	11.88	35.63
21	Fine mudstone	5	121	83.33	6.25	4.17	9.38
20	Medium sandstone	4	116	65.63	5.63	3.75	7.50
19	Sandy mudstone	5	112	85.23	2.56	5.97	9.38
18	Medium sandstone	3	107	49.22	4.22	2.81	5.63
17	Sandy mudstone	4	104	68.18	2.05	4.77	7.50
16	Medium sandstone	2	100	32.81	2.81	1.88	3.75
15	Sandy mudstone	5	98	85.23	2.56	5.97	9.38
14	Medium sandstone	5	93	82.03	7.03	4.69	9.38
13	Sandy mudstone	5	88	85.23	2.56	5.97	9.38
12	Fine sandstone	5	83	83.33	6.25	4.17	9.38
11	Sandy mudstone	16	78	272.73	8.18	19.09	30.00
10	Siltstone	4	62	66.67	5.83	2.50	7.50
9	Sandy mudstone	12	58	204.55	6.14	14.32	22.50
8	Fine sandstone	4	46	66.67	5.00	3.33	7.50
7	Siltstone	13	42	216.67	18.96	8.13	24.38
6	Medium sandstone	1	29	16.41	1.41	0.94	1.88
5	Sandy mudstone	4	28	68.18	2.05	4.77	7.50
4	Medium sandstone	10	24	164.06	14.06	9.38	18.75
3	Siltstone	6	14	105.00	7.88	18.38	13.13
2	2-2 Coal	5	8	48.21	5.63	2.41	5.63
1	Sandy mudstone	3	3	233.33	20.42	8.75	26.25
Total				2803.14	180.27	166.59	315.00

Water-rich areas exist in the coal seam roof. In order to analyze the stress evolution law before and after drainage, the no. 4 medium sandstone part in Table 1 is taken as an artesian aquifer. Several water pipes are placed in the aquifer during the building of the model. The water pipe is 2.1 m long, 1.4 m from the left boundary and 1.5 m from the right boundary of the model. The water pipe is provided with a cut-off valve, and the tail end is close to the rear steel plate for the convenience of drainage, as shown in Figure 6a. Ten UEI pressure boxes with high precision are staggered under the artesian aquifer and coal seam to monitor the stress transfer of the coal seam and roof during and after drainage, as shown in Figure 6b. The spacing between the test model and stress sensor is shown in Figure 6c.

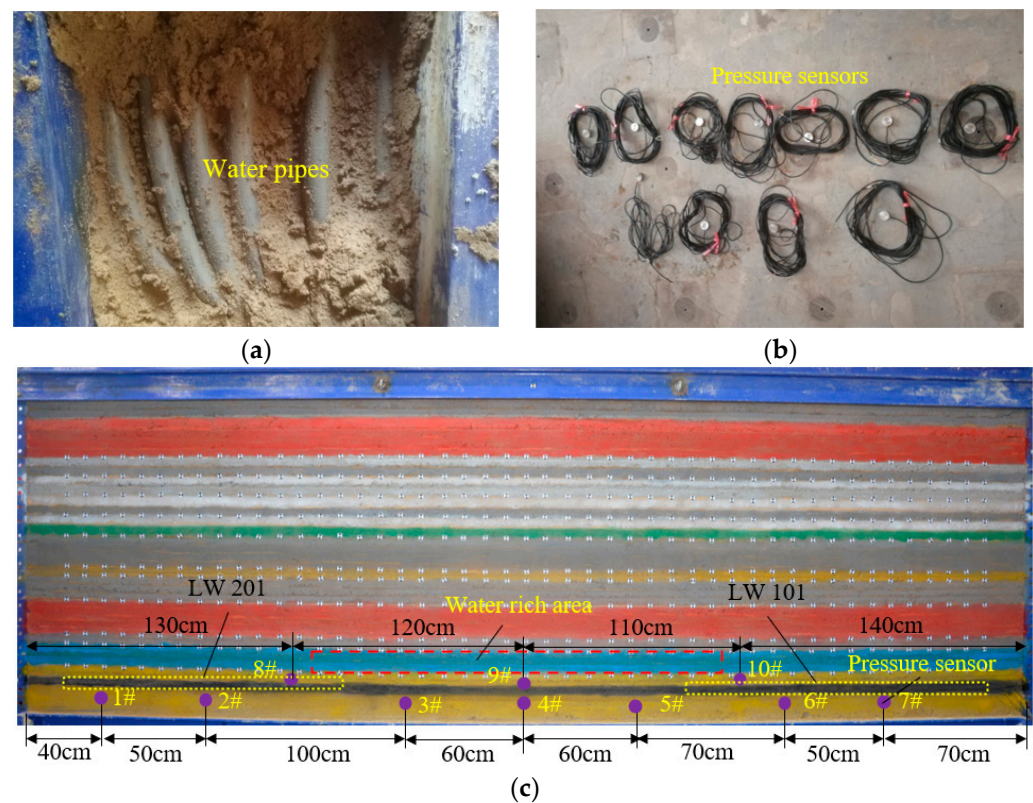


**Figure 6.** Physical simulation model: (a) water pipes laying; (b) pressure sensors; and (c) test model layout. The different numbers are stress measuring points.

In order to study the influence of water drainage on coal seam mining, a 170 cm coal pillar is set in the middle to avoid the influence of excavation on both sides of the working face. The mining sequence is as follows: (1) first, excavate LW101 from the position 20 cm to 170 cm away from the right boundary of the model, with a total length of 150 cm; (2) secondly, open the stop valve of water pipe to release all of the water, and stand for a week after the completion of water drainage; (3) finally, excavate LW201 from the position 20 cm to 160 cm away from the left boundary of the model, with a total length of 140 cm. Before the initial excavation, the stress monitoring instrument is used to clear the sensor stress to zero for comparison.

Figure 7a shows the stress changing curve of no. 8 and no. 9 measuring points after drainage. It can be seen that the stress at the no. 9 measuring point under the water-rich area shows an upward trend after drainage, with a sharp increase from the initial 0 kPa to 13 kPa between 0.5 h and 1 h after drainage, and eventually stabilizes to 16 kPa after 5 h. Meanwhile, the stress at the no. 8 measuring point at the edge of the water-rich area gradually declines from the initial 0 kPa to  $-7$  kPa after 6 h. The drainage in the water-rich area will lead to the stress change in the coal seam, namely the stress decrease under the water-rich area and the stress increase at the edge of the water-rich area, thus forming the pressurized zone and pressure relief zone. Figure 7b is the stress changing curve of no. 1~no. 4 measuring points after drainage. It can be found that no apparent stress changes have taken place at no. 1 and no. 2 measuring points after drainage, which are far away from the water-rich area, and the change has been floating up and down within the allowable error range. The stress at no. 3 and no. 4 measuring points under the water-rich area decreases from 0 kPa to  $-1.75$  kPa and from 0 kPa to  $-2$  kPa, respectively. The stress changing curve of no. 8 and no. 9 measuring points displays that the influence range affected by drainage stress will not expand indefinitely, and the stress concentration simply appears in a certain range at the edge of the water-rich area.

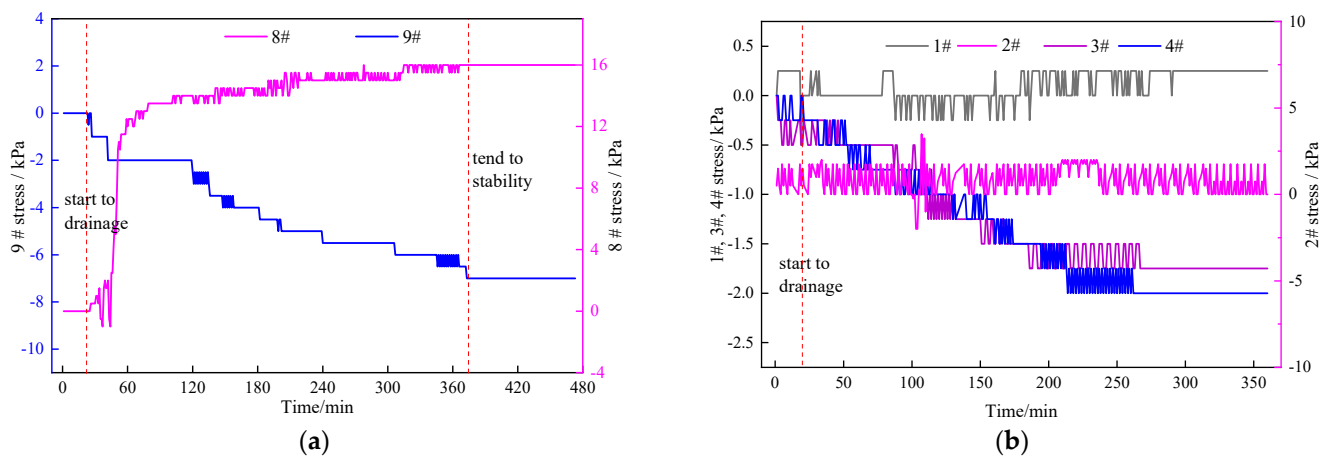


Figure 7. Stress changing curves of each measuring point after drainage: (a) no. 8, no. 9; and (b) no. 1–no. 4.

Figure 8a shows the stress changing curves at the no. 6 measuring point with LW101 excavated for 90~95 cm and at the no. 2 measuring point with LW201 excavated for 60~65 cm. At this time, the no. 6 measuring point is 100 cm away from the open cutting of LW101 and 5 cm away from the advancing position of LW101; the no. 2 measuring point is 70 cm away from the open cutting hole of LW201 and 5 cm away from the advancing position of LW201. It can be seen that the two measuring points basically keep a consistent stress growth trend, and the initial stress of the no. 2 measuring point is only 2.5 kPa lower than that of the no. 6 measuring point, which is within the allowable error range of the instrument.

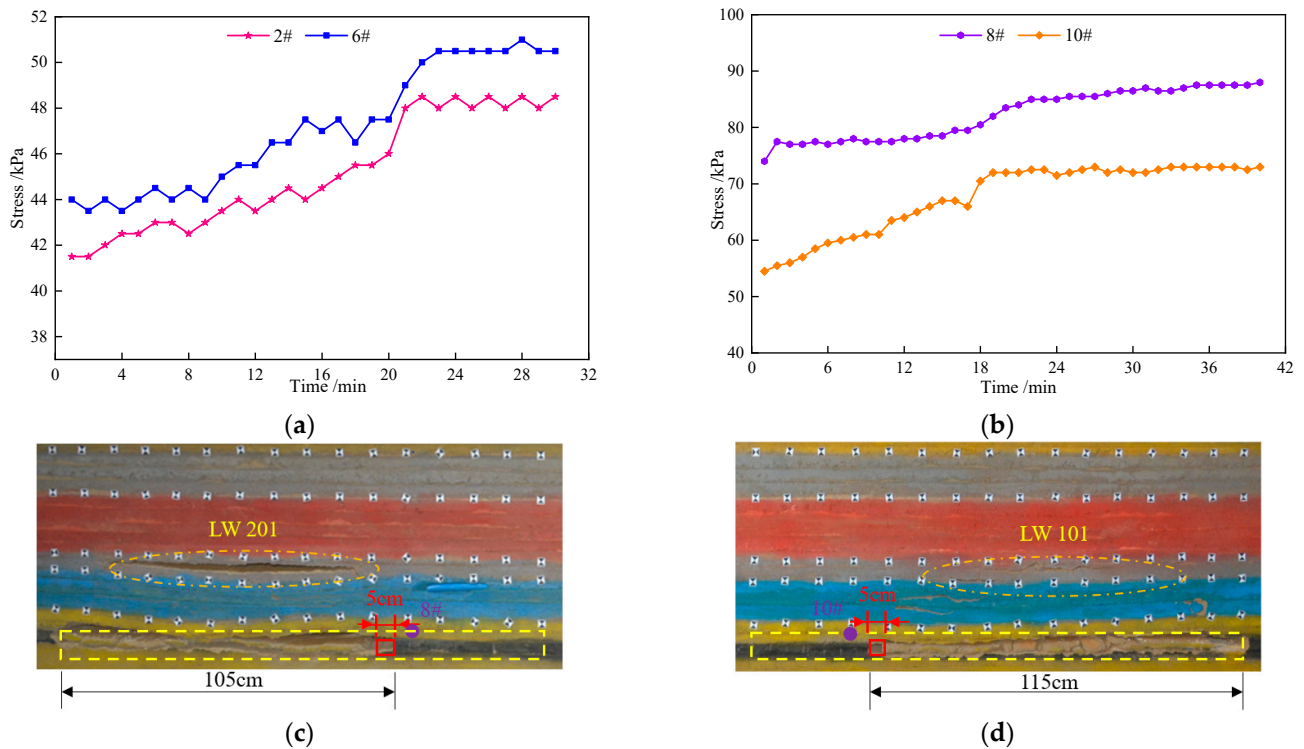


Figure 8. Stress changing curve of each measuring point during mining: (a) no. 2, no. 6; (b) no. 8, no. 10; (c) excavation location of LW201, no. 6; and (d) excavation location of LW101.

Figure 8b shows the stress changing curves at the no. 10 measuring point with LW101 excavated for 110~115 cm and at the no. 8 measuring point with LW201 excavated for

100~105 cm. At this time, the no. 10 measuring point is 120 cm distant from the open cutting of LW101 and 5 cm from the advancing position of LW101; the no. 8 measuring point is 110 cm from the open cutting hole of LW201 and 5 cm from the advancing position of LW201. It can be obtained that the two measuring points almost present the same stress growth trend, and the initial stress of the no. 8 measuring point is 19.5 kPa higher than that of the no. 10 measuring point. When the two working faces are advanced to 5 cm away from the measuring point, the stress of the no. 8 measuring point is 15 kPa higher than that of the no. 10 measuring point. The stress difference is similar to the stress increment of 16 kPa at the no. 8 measuring point after drainage in Figures 7a and 8c,d demonstrates the spatial relationship between the working face and the stress measuring point when LW101 is excavated for 110~115 cm and LW201 for 100~105 cm.

Above all, the influence range of drainage stress will not expand indefinitely, and stress concentration only appears in a certain range at the edge of the water-rich area. Compared with the working face not affected by water drainage, when the working face advances to the drainage-affected area, the mining disturbance stress and drainage transfer stress will be superimposed. If the superimposed stress reaches the critical stress, rock burst will be induced, which verifies the correctness of the theoretical calculation model.

### 3.4. Analysis of the Relationship between Drainage and Rock Burst

In order to evaluate the rock burst risk at point  $N$ , the rock burst risk evaluation index  $I_c$  [42] proposed by our research team is introduced.  $I_c$  stands for the ratio of vertical stress at point  $N$  to the uniaxial compressive strength of coal rock mass, expressed as:

$$I_c = \frac{\sigma_N}{[\sigma_c]} \quad (9)$$

where  $\sigma_N$  is the vertical stress at point  $N$  and  $[\sigma_c]$  is the uniaxial compressive strength of coal rock mass. The classification of rock burst risk is shown in Table 2.

**Table 2.** Relationship between  $I_c$  and rock burst risk.

$I_c$	<1.5	1.5~2.0	2.0~2.5	>2.5
Rock burst risk	None	Weak	Medium	Powerful

In the mining process of the roof water drainage working face, the superimposed stress on the coal body varies according to the position of point  $N$  (as shown in Figure 9).

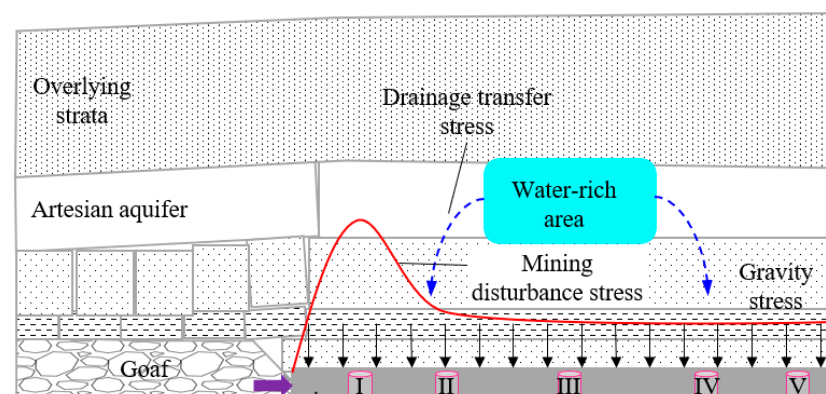


**Figure 9.** Stress environment of coal body at a certain point in the mining process of roof water drainage working face. The I–V is the position of point  $N$ .

The following situations typically exist: (1) affected by gravity stress and mining disturbance stress (I, V); (2) affected by gravity stress and pressure relief from drainage and pressurization from mining disturbance under the water-rich area; and (3) affected by

gravity stress and pressurization from drainage and mining disturbance at the edge of the water-rich area (II, IV). The stress state at point  $N$  can be approximated as:

$$\sigma_N = q + [\sigma_M - q] + [\sigma_S(x) - q] = \sigma_M + \sigma_S(x) - q \quad (10)$$

where  $\sigma_N$  is the superimposed stress at point  $N$ ,  $\sigma_M$  is the mining disturbance stress at point  $N$ , and  $x$  is the horizontal distance between point  $N$  and the center of the water-rich area.

According to Formula (10), the vertical stress at point  $N$  is related to the mining speed and the drainage degree. When it is affected by both drainage pressurization and mining disturbance pressurization, the stress condition of rock burst induction can easily be reached.

The above analysis explains the rock burst mechanism induced by water drainage in the roof water-rich area of deep mines. That is to say, when the working face is passing the pressurization area by drainage, the coal rock mass is under the combined influence of gravity stress, mining disturbance stress and drainage transfer stress, and the superimposed stress easily exceeds the critical value of rock burst, which is the main reason to induce rock burst.

#### 4. Field Application and Verification

##### 4.1. Field Application

Water drainage is taken before mining on LW21106. Water pressure in the water-rich area decreases from 3 MPa at the beginning to 0.5 MPa after drainage. After the drainage is completed, the pressure relief zone and pressurized zone are formed in front of the working face, which facilitates the changes in the rock burst risk areas on the working face. In this case, the rock burst risk areas can be re-predicted and divided according to the location of risk areas.

Due to the weak rock burst liability of seam 2-2 in the Shilawusu Mine, the rock burst risk assessment of LW22106 has been carried out before mining. Field practice and research show that the peak value of mining disturbance stress is generally 1.5~1.8 times the original rock stress under the condition of a constant mining speed. It can be calculated that the peak value of mining disturbance stress is about 24.75~29.7 MPa with an average of 27.225 MPa, and the rock burst risk index  $I_c = 27.225/17.6 = 1.55$ . Thus, the working face is determined to have a weak rock burst risk. Taking the no. 4 water-rich area as an example, the multi-factor coupling evaluation method is adopted to divide the rock burst risk areas around the no. 4 water-rich area, including three weak rock burst risk areas and one medium rock burst risk area, as shown in Figure 10 and Table 3.

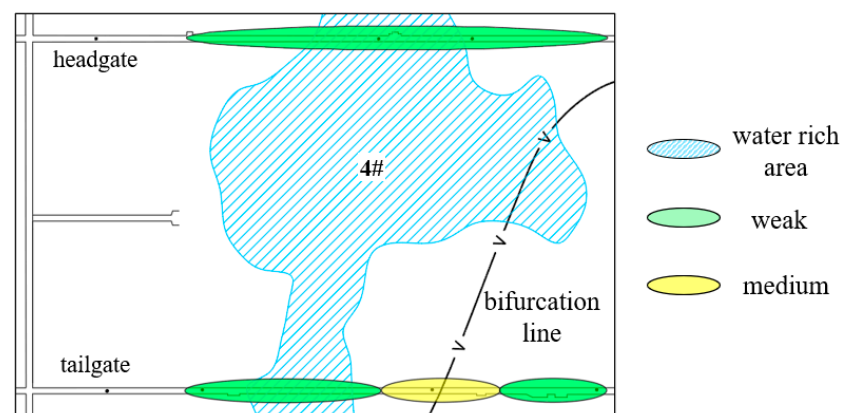


Figure 10. Division diagram of rock burst risk areas around no. 4 water-rich area before drainage.

**Table 3.** Division table of rock burst risk areas around no. 4 water-rich area before drainage.

Location	Serial Number	Range/m	Main Factors	Risk Degree of Rock Burst
Headgate	1	740~1100	Depth, mining disturbance	Weak
	2	Distance from open-off cut	740~830	Depth, mining disturbance
Tailgate	3	830~930	Depth, mining disturbance, bifurcation of coal	Medium
	4	930~1100	Depth, mining disturbance	Weak

However, the evaluation result does not take into account the influencing factors of drainage in the water-rich area. Therefore, it can be believed that the evaluation result is a classification method of rock burst risk areas simply considering the mining disturbance before drainage.

After the completion of water drainage, the pressure relief zone and pressurized zone are formed in front of the working face, which results in the change in the rock burst risk areas on the working face. According to the actual situation of LW22106, the values are as follows:  $h_1 = 160$  m, where  $h_1$  is defined as the distance from the top of the artesian aquifer to the coal seam;  $h_2 = 500$  m, where  $h_2$  represents the distance from the surface to the top of the artesian aquifer;  $2l_1 = 40$  m, where  $2l_1$  refers to the average width of the narrow area in the no. 4 water-rich area;  $2l_1 = 260$  m, where  $2l_1$  is the average width of the wide area;  $\alpha = 86^\circ$ , where  $\alpha$  means the fracture angle of the overlying strata in the water-rich area after drainage;  $k = 0.8$ , where  $k$  is taken as the pressure relief coefficient (the water pressure in the water-rich area is reduced from the initial 3 MPa to 0.5 MPa after drainage, which reports that the pressure relief value is about 20% of the original stress of water-rich artesian aquifer, so  $k = 1 - 0.2 = 0.8$ );  $[\sigma_c] = 17.6$  MPa, where  $[\sigma_c]$  stands for the uniaxial compressive strength of coal; and  $\gamma = 25$  kN/m<sup>3</sup>. By substituting each parameter into Equation (8), it can be obtained that the stress influence range after drainage is about 35 m, the peak value is about 17.5 m away from the edge of the water-rich area, the stress peak value is 33.4 MPa in the narrow zone of the no. 4 water-rich area, and the stress peak value is 46.3 MPa in the wide zone of the no. 4 water-rich area.

Given the mining disturbance stress and the stress transfer before and after drainage in the no. 4 water-rich area, it can be obtained that:

When the working face is advanced to the pressurized zone in the no. 4 water-rich area, the stress peak value  $\sigma_{N_{\max 1}} = 27.225 + 33.4 - 16.5 = 44.125$  Mpa,  $I_c = 2.51$ ,  $\sigma_{N_{\max 2}} = 27.225 + 46.3 - 16.5 = 57.025$  Mpa and  $I_c = 3.24$ . It can be comprehensively determined that the working face has a powerful rock burst risk at this time.

When the working face is advanced to the pressure relief zone in the no. 4 water-rich area, the stress peak value  $\sigma_{M_{\max 3}} = 27.225 + 14 - 16.5 = 24.725$  MPa and  $I_c = 1.40$ , which indicates there is no rock burst risk on the working face at this time.

It can be seen that it is easy to induce the rock burst when the working face is advanced to the pressurized zone, which is also consistent with the rock burst location on 10 October. On this basis, the rock burst risk areas after drainage are re-predicted and re-divided for the surrounding area of the no. 4 water-rich area, including two no rock burst risk areas, four weak rock burst risk areas, one medium rock burst risk area and six powerful rock burst risk areas, as shown in Figure 11 and Table 4.

By comparing Figures 10 and 11 and Tables 3 and 4, it can be obtained that the number of risk areas increases from 4 before drainage to 13 after drainage, one in-plane rock burst risk area is added, and the risk degrees change from weak and moderate rock burst before drainage to no, weak, medium and powerful rock burst after drainage. It can also be found that the pressurized zone and the pressure relief zone on the working face and two gate roads before and after drainage in the water-rich area lead to great changes in the rock burst risk zones and risk degrees on the working face. The rock burst risk degree is remarkably reduced within the pressure relief zone, whereas it significantly increases in the pressurized zone. All rock burst locations on 10 October 2019 are in the no. 13 in-plane

pressurized zone, which further demonstrates that the division of the rock burst risk areas on the working face after drainage is extremely consistent with the field practice.

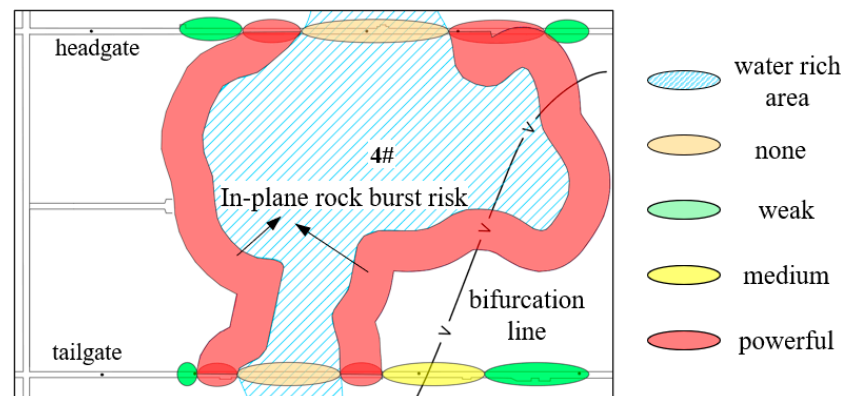


Figure 11. Division diagram of rock burst risk areas around no. 4 water-rich area after drainage.

Table 4. Division table of rock burst risk areas around no. 4 water-rich area after drainage.

Location	Serial Number	Range/m	Main Factors	Risk Degree of Rock Burst
Headgate	1	740~780	Depth, mining disturbance	Weak
	2	Distance from open-off cut 780~862	Depth, mining disturbance drainage pressurization	Powerful
	3	862~988	Depth, mining disturbance drainage pressure relief	None
	4	988~1038	Depth, mining disturbance drainage pressurization	Powerful
	5	1038~1100	Depth, mining disturbance	Weak
	6	740~830	Depth, mining disturbance	Weak
Tailgate	7	Distance from open-off cut 830~918	Depth, mining disturbance Bifurcation of coal	Medium
	8	918~953	Depth, mining disturbance bifurcation of coal, drainage pressurization	Powerful
	9	953~1043	Depth, mining disturbance drainage pressure relief	None
	10	1043~1078	Depth, mining disturbance drainage pressurization	Powerful
In-plane	11	1078~1100	Depth, mining disturbance	Weak
	12	no. 4 water rich area Right side 0~35	Depth, mining disturbance drainage pressurization	Powerful
	13	Left side 0~35	Depth, mining disturbance drainage pressurization	Powerful

#### 4.2. Field Verification

Each microseismic event has rich temporal and spatial information [43]. Real-time monitoring and processing of microseismic events can identify the occurrence location and intensity of microseismic events, further determining the stress transition inside coal rock masses. Figure 12 shows the relationship between daily footage and daily microseismic energy of LW22106 from 1 September 2019 to 23 October 2019. Figure 13 is the plane projection of microseismic events above the 4th power of LW22106 during this period. It can be seen that mining Zone I from 1 September to 9 September was partly under the water-rich area and partly outside the influence range of drainage, and the microseismic energy just had a small change with the increase in mining speed. From 10 September to 18 September, mining Zone II was partly under the water-rich area and partly within the pressurized zone, and the microseismic energy increased significantly at a high mining

speed compared with Zone I. Mining Zone III from 19 September to 4 October was almost under the water-rich area, and the microseismic energy was still very small in spite of a high mining speed (maximum 8.8 m/d). From 5 October to 14 October, most of mining Zone IV was within the pressurized zone, and the high mining speed resulted in the maximum daily energy and a significant increase in total microseismic energy. Most of mining Zone V from 15 October to 23 October was not affected by water drainage, and the microseismic energy was changed little with the changing mining speed. The red line in Figure 13 represents the footage of the working face. It can be found that the microseismic events mostly occurred within the pressurized zone, which proved that this zone had a high degree of concentration with the working face being advanced here. Therefore, rock burst appeared on the working face on 10 October.

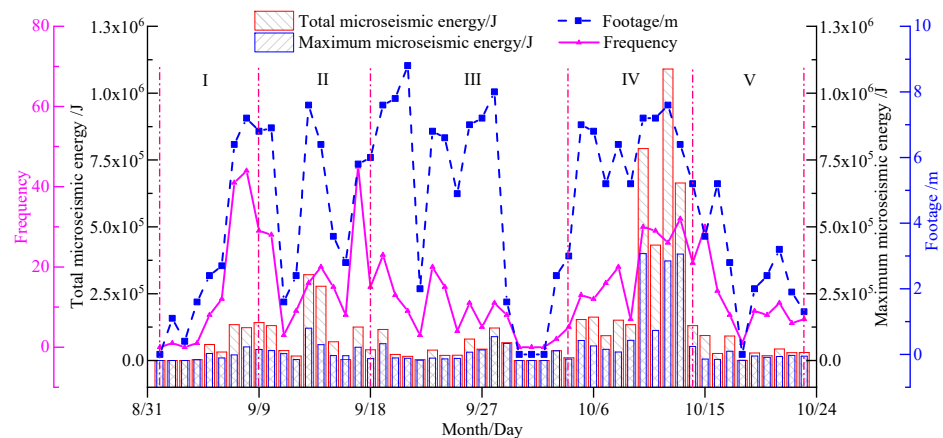


Figure 12. Curves of daily advance and microseismic energy.

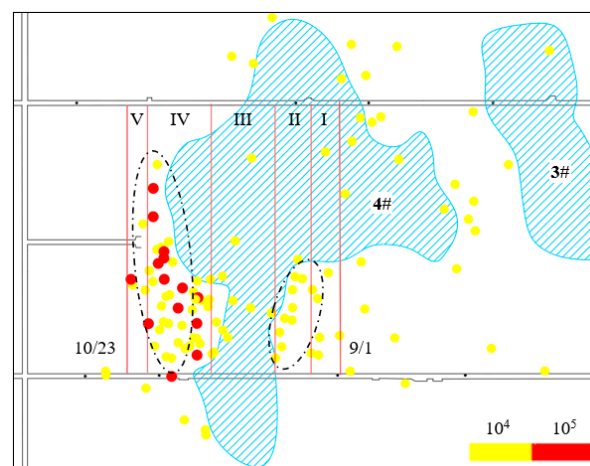


Figure 13. Plane projection of microseismic events above the 4th power of LW22106.

Reducing the mining speed can lower the peak of advanced abutment pressure and the overhanging distance of the basic roof, thus providing reserved time for rock energy release and decreasing the deformation rate of surrounding rock. However, a blind decrease in mining speed will cause huge economic losses. Taking into account the social resource utilization, corporate economic development and safety production, the dynamic control of the mining speed is suggested in the areas affected by water drainage.

In the mining process, according to the mining situation in the normal areas (no fault, no water-rich and other stress abnormal areas), the pressure step distance and preliminary reasonable mining speed can be determined through the microseismic statistical curve and theoretical calculation. When the working face is passing the pressurized zone, the mining speed should be reduced to ensure the stress peak cannot meet the condition of inducing

rock burst. The mining speed can be increased appropriately within the pressure relief zone, but the superimposed stress should not reach the critical value of rock burst.

## 5. Conclusions

Taking the roof water-rich LW22106 of the Shilawusu Mine in Ordos as the engineering background, this paper investigates the occurrence mechanism of rock burst induced by water drainage in deep mines through theoretical analysis, similar material simulation and microseismic monitoring and draws the following main conclusions:

(1) The influence range of drainage stress does not expand indefinitely. A stress concentration just appears within a certain range at the edge of the water-rich area and tends to have been stable during mining on the working face. The pressure relief zone, pressurized zone and pressure stabilization zone are formed in sequence from the center to both sides. The width of the pressure relief zone is consistent with that of the water-rich area, and the width of the pressurized zone is about 35 m on one side. The pressurized zone applies additional stress to the coal seam and its roof, adding a static stress source for the occurrence of rock burst.

(2) During the forward mining process on the roof water drainage working face, the stress environment is different due to the different positions of a certain point  $N$  in coal. When the mining is passing the pressurized zone, the coal rock mass is under the joint influence of gravity stress, mining disturbance stress and drainage transfer stress. The superimposed stress generally exceeds 2.5 times (UCS) the coal rock mass, and the maximum reaches 3.24 times that, far exceeding the critical value of rock burst (1.5 times UCS), which is the main reason for inducing rock burst.

(3) By calculating the stress distribution of the drainage-affected zone in the no. 4 water-rich area on the working face, the dynamic change in the rock burst risk areas before and after drainage has been predicted. The number of risk areas increases from 4 before drainage to 13 after drainage, and the in-plane rock burst risk areas are added. The risk degrees change from weak and moderate rock burst before drainage to no, weak, medium and powerful rock burst after drainage. The effect of stress superposition caused by different mining speeds is different. Therefore, it is proposed that the dynamic regulation of mining speed in front and at the back of the drainage area is an effective and efficient method for rock burst prevention and control. That is to say, the mining speed should be dynamically adjusted on the basis of the theoretical analysis and microseismic monitoring results.

This paper attempts to provide mine researchers and designers a classification method of the rock burst risk areas with consideration of drainage so as to predict the rock burst risk of drainage working faces in a more accurate way. However, the current research does not take into consideration the influence of dynamic drainage on the strength of coal rock masses. Further studies on how drainage affects the macro- and microstructures and mechanical properties of coal rock masses are still needed.

**Author Contributions:** Conceptualization, B.W. and G.F.; methodology, F.J. and Z.L.; formal analysis, B.W. and Z.L.; investigation, G.F. and W.W.; resources, J.M. and C.W.; writing—original draft preparation, B.W.; writing—review and editing, B.W. and G.F.; visualization, F.J.; funding acquisition, B.W. and G.F. All authors have read and agreed to the published version of the manuscript.

**Funding:** This research was funded by the National Natural Science Foundation of China, grant no. 52204107 and no. U22A20169; the Fundamental Research Program of Shanxi Province, grant no. 202103021223072; and the Tencent Foundation or Xplorer Prize.

**Institutional Review Board Statement:** Not applicable.

**Informed Consent Statement:** Not applicable.

**Data Availability Statement:** The data involved in this paper are all included in the text of the manuscript.

**Acknowledgments:** Special thanks should be extended to the Shilawusu Coal Mine for the provided raw data. The authors thank the anonymous reviewers for constructive comments that helped to improve the quality of the paper.

**Conflicts of Interest:** The authors declare no conflict of interest.

## References

- Xie, H.P.; Ju, Y.; Ren, S.H.; Gao, F.; Liu, J.Z.; Zhu, Y. Theoretical and technological exploration of deep in situ fluidized coal mining. *Front. Energy* **2019**, *13*, 603–611. [[CrossRef](#)]
- Jiang, Y.D.; Pan, Y.S.; Jiang, F.X.; Dou, L.M.; Ju, Y. State of the art review on mechanism and prevention of coal bumps in China. *J. China Coal Soc.* **2014**, *39*, 205–213.
- Pan, Y.S. Disturbance response instability theory of rockburst in coal mine. *J. China Coal Soc.* **2018**, *43*, 2091–2098.
- Li, J.Z.; Li, S.Y.; Ren, W.T.; Liu, H.; Liu, S.; Yan, K.X. Seismic reduction mechanism and engineering application of paste backfilling mining in deep rock burst mines. *Sustainability* **2023**, *15*, 4336. [[CrossRef](#)]
- Qi, Q.X.; Wang, S.G.; Li, H.T.; Mu, P.Y.; Du, W.S.; Yang, G.Y. Stress flow theory for coal bump and its numerical implementation. *J. China Coal Soc.* **2022**, *47*, 172–179.
- He, M.C.; Zhao, F.; Cai, M.; Du, S. A novel experimental technique to simulate pillar burst in laboratory. *Rock Mech. Rock Eng.* **2015**, *48*, 1833–1848. [[CrossRef](#)]
- Bräuner, G. *Rockbursts in Coal Mines and Their Prevention*; Routledge: Abingdon, UK, 2017.
- Gu, S.T.; Chen, H.X.; Li, W.S.; Jiang, B.Y.; Chen, X. Study on occurrence mechanism and prevention technology of rock burst in narrow coal pillar working face under large mining depth. *Sustainability* **2022**, *14*, 15435. [[CrossRef](#)]
- Das, A.J.; Mandal, P.K.; Paul, P.S.; Sinha, R.K. Generalised Analytical Models for the Strength of the Inclined as well as the Flat Coal Pillars using Rock Mass Failure Criterion. *Rock Mech. Rock Eng.* **2019**, *52*, 3921–3946. [[CrossRef](#)]
- Gao, R.; Kuang, T.J.; Zhang, Y.Q.; Zhang, W.Y.; Quan, C.Y. Controlling mine pressure by subjecting high-level hard rock strata to ground fracturing. *Int. J. Coal Sci. Technol.* **2021**, *8*, 1336–1350. [[CrossRef](#)]
- Vizintin, G.; Kocjancic, M.; Vulic, M. Study of coal burst source locations in the velenje colliery. *Energies* **2016**, *9*, 507. [[CrossRef](#)]
- Dong, S.N.; Ji, Y.D.; Wang, H.; Zhao, B.F.; Cao, H.D.; Liu, Y.; Liu, Y.F.; Ji, Z.K.; Liu, B.G. Prevention and control technology and application of roof water disaster in Jurassic coal field of Ordos Basin. *J. China Coal Soc.* **2020**, *45*, 2367–2375.
- Dong, S.N.; Wang, H.; Guo, X.M.; Zhou, Z.F. Characteristics of water hazards in China’s coal mines: A review. *Mine Water Environ.* **2021**, *40*, 325–333. [[CrossRef](#)]
- Wang, B.; Jiang, F.X.; Zhu, S.T.; Zhang, X.F.; Shang, X.G.; Gu, Y.S.; Wu, Z. Investigating on the mechanism and prevention of rock burst induced by high intensity mining of drainage area in deep mines. *J. China Coal Soc.* **2020**, *45*, 3054–3064.
- Jiang, Y.D.; Wang, H.W.; Xue, S.; Zhao, Y.X.; Zhu, J.; Pang, X.F. Assessment and mitigation of coal bump risk during extraction of an island longwall panel. *Int. J. Coal Geol.* **2012**, *95*, 20–33. [[CrossRef](#)]
- Dou, L.M.; He, J.; Cao, A.Y.; Gong, S.Y.; Cai, W. Rock burst prevention methods based on theory of dynamic and static combined load induced in coal mine. *J. China Coal Soc.* **2015**, *40*, 1469–1476.
- Dou, L.M.; Cai, W.; Cao, A.Y.; Guo, W.H. Comprehensive early warning of rock burst utilizing microseismic multi-parameter indices. *Int. J. Rock Mech. Min. Sci.* **2018**, *28*, 767–774. [[CrossRef](#)]
- Cai, W.; Dou, L.M.; Si, G.Y.; Hu, Y.W. Fault-Induced coal burst mechanism under mining-induced static and dynamic stresses. *Engineering* **2021**, *7*, 687–700. [[CrossRef](#)]
- Qi, Q.X.; Pan, Y.S.; Li, H.T.; Jiang, D.Y.; Shu, L.Y.; Zhao, S.K.; Zhang, Y.J.; Pan, J.F.; Li, H.Y.; Pan, P.Z. Theoretical basis and key technology of prevention and control of coal-rock dynamic disasters in deep coal mining. *J. China Coal Soc.* **2020**, *45*, 1567–1584.
- Jiang, F.X.; Liu, Y.; Zhang, Y.C.; Wen, J.L.; Yang, W.L.; An, J. A three-zone structure loading model of overlying strata and its application on rockburst prevention. *Chin. J. Rock Mech. Eng.* **2016**, *35*, 2398–2408.
- Zhu, S.T.; Feng, Y.; Jiang, F.X. Determination of abutment pressure in coal mines with extremely thick alluvium stratum: A typical kind of rock burst mines in china. *Rock Mech. Rock Eng.* **2016**, *49*, 1943–1952. [[CrossRef](#)]
- Zhu, S.T.; Feng, Y.; Jiang, F.X.; Liu, J.H. Mechanism and risk assessment of overall-instability-induced rockbursts in deep island longwall panels. *Int. J. Rock Mech. Min. Sci.* **2018**, *106*, 342–349. [[CrossRef](#)]
- Zhao, Y.X.; Zhou, J.L.; Liu, W.G. Characteristics of ground pressure and mechanism of coal burst in the gob side roadway at Xinjie deep mining area. *J. China Coal Soc.* **2020**, *45*, 1595–1606.
- Cao, A.Y.; Dou, L.M.; Wang, C.B.; Yao, X.X.; Dong, J.Y.; Gu, Y. Microseismic precursory characteristics of rock burst hazard in mining areas near a large residual coal pillar: A case study from Xuzhuang coal mine, Xuzhou, China. *Rock Mech. Rock Eng.* **2016**, *49*, 4407–4422. [[CrossRef](#)]
- Cao, A.Y.; Dou, L.M.; Cai, W.; Gong, S.Y.; Liu, S.; Jing, G.C. Case study of seismic hazard assessment in underground coal mining using passive tomography. *Int. J. Rock Mech. Min. Sci.* **2015**, *78*, 1–9. [[CrossRef](#)]
- Cao, A.Y.; Liu, Y.Q.; Chen, F.; Hao, Q.; Yang, X.; Wang, C.B.; Bai, X.X. Focal mechanism and source parameters analysis of mining-induced earthquakes based on relative moment tensor inversion. *Int. J. Environ. Res. Public Health* **2022**, *19*, 7352. [[CrossRef](#)]
- Gong, F.Q.; Zhang, P.L.; Luo, S.; Li, J.C.; Huang, D. Theoretical damage characterisation and damage evolution process of intact rocks based on linear energy dissipation law under uniaxial compression. *Int. J. Rock Mech. Min. Sci.* **2021**, *146*, 104858. [[CrossRef](#)]
- Gong, F.Q.; Zhong, W.H.; Gao, M.Z.; Si, X.F.; Wu, W.X. Dynamic characteristics of high stressed red sandstone subjected to unloading and impact loads. *J. Cent. South Univ.* **2022**, *29*, 596–610. [[CrossRef](#)]

29. Zhao, T.B.; Guo, W.Y.; Han, F.; Gu, S.T. Analysis on energy accumulation and release of roof under influence of mining speed. *Coal Sci. Technol.* **2018**, *46*, 37–44.
30. Huang, B.X.; Liu, J.W. The effect of loading rate on the behavior of samples composed of coal and rock. *Int. J. Rock Mech. Min. Sci.* **2013**, *61*, 23–30. [[CrossRef](#)]
31. Cui, F.; Zhang, T.H.; Lai, X.P.; Wang, S.J.; Chen, J.Q.; Qian, D.Y. Mining disturbance characteristics and productivity of rock burst mines under different mining intensities. *J. China Coal Soc.* **2021**, *46*, 3781–3793.
32. Feng, L.F.; Dou, L.M.; Wang, X.D.; Jin, D.W.; Cai, W.; Xu, G.G.; Jiao, B. Mechanism of mining advance speed on energy release from hard roof movement. *J. China Coal Soc.* **2019**, *44*, 3329–3339.
33. Zhou, K.Y.; Dou, L.M.; Song, S.K.; Ma, X.T.; Chen, B.G. Experimental Study on the mechanical behavior of coal samples during water saturation. *ACS Omega* **2021**, *6*, 33822–33836. [[CrossRef](#)]
34. Zheng, L.W.; Dong, S.N.; Tang, S.L.; Ji, Y.D.; Luo, J.Z.; Li, H.H.; Li, X.L.; Liu, C.Y.; Zeng, M.L. Molecular structure characterization of coal under the water-rock interaction in acid mine drainage (AMD). *J. Mol. Struct.* **2022**, *1251*, 132043.
35. Zhang, C.; Bai, Q.S.; Han, P.H.; Wang, L.; Wang, X.J.; Wang, F.T. Strength weakening and its micromechanism in water-rock interaction, a short review in laboratory tests. *Int. J. Coal Sci. Technol.* **2023**, *10*, 10. [[CrossRef](#)]
36. Han, P.H.; Zhang, C.; Wang, X.J.; Wang, L. Study of mechanical characteristics and damage mechanism of sandstone under long-term immersion. *Eng. Geol.* **2023**, *315*, 107020. [[CrossRef](#)]
37. Zhang, C.; Bai, Q.S.; Han, P.H. A review of water rock interaction in underground coal mining: Problems and analysis. *Bull. Eng. Geol. Environ.* **2023**, *82*, 157.
38. Cao, A.Y.; Chen, F.; Liu, Y.Q.; Dou, L.M.; Wang, C.B.; Yang, X.; Bai, X.X.; Song, S.K. Response characteristics of rupture mechanism and source parameters of mining tremors in frequent coal burst area. *J. China Coal Soc.* **2022**, *47*, 722–733.
39. Li, D.; Jiang, F.X.; Chen, Y.; Shu, C.X.; Tian, Z.J.; Wang, Y.; Wang, W.B. Mechanism of rockburst induced by “dynamic-static” stress effect in water-rich working face of deep well. *Chin. J. Geo. Eng.* **2018**, *40*, 1714–1722.
40. Du, X.L.; Zhang, P.; Xu, C.S.; Lu, D.C. On principle of effective stress and effective stress. *Chin. J. Geo Eng.* **2018**, *40*, 486–494.
41. Li, Z.; Yu, S.C.; Zhu, W.B.; Feng, G.R.; Xu, J.M.; Guo, Y.X.; Qi, T.Y. Dynamic loading induced by the instability of voussoir beam structure during mining below the slope. *Int. J. Rock Mech. Min. Sci.* **2020**, *132*, 104343.
42. Wang, J.C.; Jiang, F.X.; Meng, X.J.; Wang, X.Y.; Zhu, S.T.; Feng, Y. Mechanism of rock burst occurrence in specially thick coal seam with rock parting. *Rock Mech. Rock Eng.* **2016**, *49*, 1953–1965. [[CrossRef](#)]
43. Hosseini, N. Evaluation of the rock burst potential in longwall coal mining using passive seismic velocity tomography and image subtraction technique. *J. Seismol.* **2017**, *21*, 1101–1110. [[CrossRef](#)]

**Disclaimer/Publisher’s Note:** The statements, opinions and data contained in all publications are solely those of the individual author(s) and contributor(s) and not of MDPI and/or the editor(s). MDPI and/or the editor(s) disclaim responsibility for any injury to people or property resulting from any ideas, methods, instructions or products referred to in the content.